

IN THE UNITED STATES PATENT AND TRADEMARK OFFICE

Serial No. : **10/531466**  
Applicant : Venturelli  
Filing date : April 15, 2005  
Title : Pipe Having at Least a Portion with a Variable Flexibility  
TC/A.U. : 4158  
Examiner : Patel  
Docket No. : **5625**  
Customer No. : 26936

---

Commissioner for Patents  
P.O. Box 1450  
Alexandria, Virginia 22313-1450

**DECLARATION OF ACHILLE SINA AND MARCO MILIANI**

**(37 C.F.R. 1.132)**

We, Achille Sina and Marco Miliani, declare that:

Our professional qualifications are attached as appendices A and B.

We have performed a finite element analysis (FEA) of two tubes, one constructed according to claim 20 (which is attached as Appendix C), the other being identical but without holes at the ends of the slots. The results of the analysis are set out below.

## Introduction

The aim of this finite element analysis (FEA) is to compare two different hypotube designs with notches cut in the hypotube wall. The comparison has been done in terms of mechanical properties and functional features of the same hypotube, having two different kind of notches.

## 1. MODELS

### 1.1 Creation of the 3D models of the hypotubes

The hypotubes under investigation have different kind of notches cut in the hypotube wall; these notches are obtained by laser cutting of hollow cylinders. The three-dimensional CAD models of the structures were built using the software 'SolidWorks' (Dassault Systèmes SolidWorks Corporation). The models have been defined starting from the 2D drawing of one of the hypotubes used on coronary products manufactured by Invatec S.p.A. and actually on the Market in a version without any notch. Two different 3D models of the hypotube have been developed in order to evaluate the influence of different notch cutting designs: the first model has simple notches cut in the hypotube wall ("simple-notches" version); the second one has notches with rounded ends ("rounded-notches" version). Both of the 3D CAD models defined are shown in Figure 1 below, in an undeformed shape.

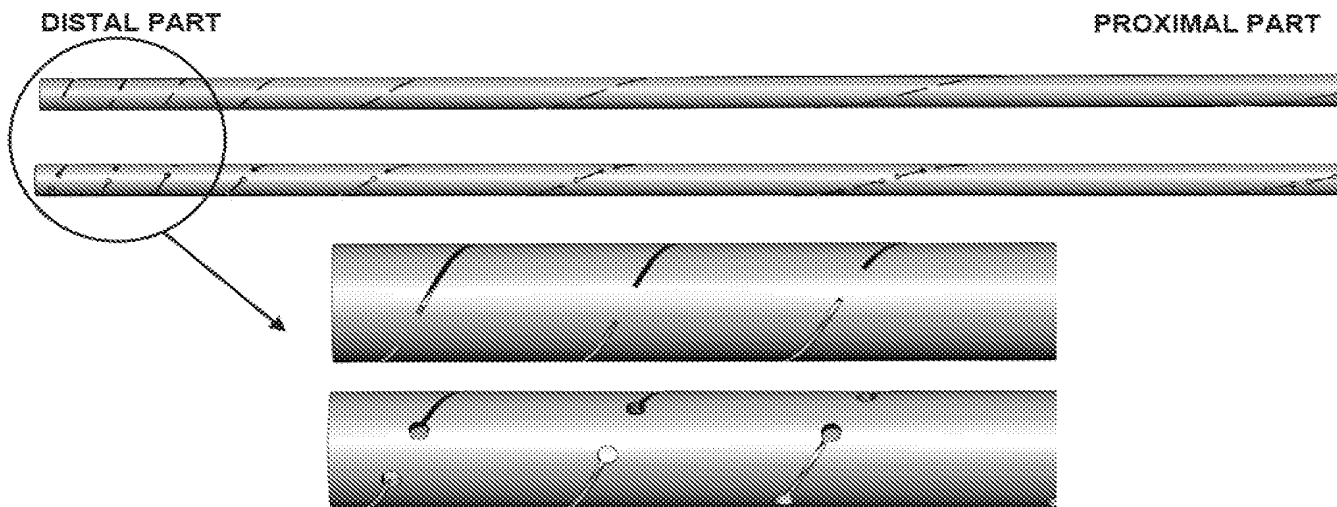


Figure 1. Two versions of the 3D CAD model with simple notches (upper) and with notches having rounded ends (lower): lateral views and zoom on distal parts.

The two models represent a portion of the hypotube mounted on an intravascular Invatec device. They are characterized by the same internal and external diameters (ID = 0.48 mm; OD = 0.64 mm) and length (24.6 mm). In the two models the notches have the same width (0.025 mm), the same distance from each another (0.21 mm) and the notches are cut in the same positions on the hypotube wall, in both of the models. The notches are cut following a spiral having an increasing pitch, from the distal to the proximal part of the hypotube. The only difference between the two models is the presence/absence of rounded ends of the notches (with a radius of 0.05 mm).

## 1.2 Mesh creation

The mesh generation and the finite element analysis has been performed using 'Simulation Xpress' software (SolidWorks - Dassault Systèmes SolidWorks Corporation). The mesh generated for the hypotube geometry was made of 3D deformable tetrahedral elements with 10 nodes each (see Figure 2).

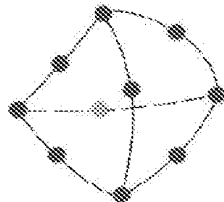


Figure 2. Detail of the tetrahedral mesh used.

The number of nodes, elements, degrees of freedom (D.O.F.) and mean element dimension for each mesh of the hypotubes is summarized in Table 1, while images of the meshed geometries are shown in Figure 3 below.

	<i>nodes</i>	<i>elements</i>	<i>D.O.F.</i>	<i>mean element dimension [mm]</i>
"simple-notches" version	64359	32620	192699	0.094625
"rounded-notches" version	75561	38500	226305	0.094435

Table 1. Element and node numbers of the mesh of the different stent geometries.

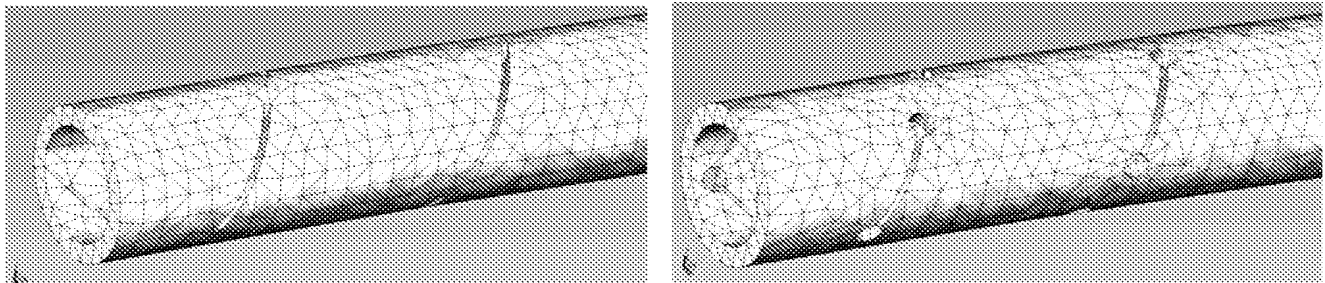


Figure 3. Detail of the tetrahedral mesh used. On the left the "simple-notches" version, on the right the "rounded-notches" version.

### 1.3 Mechanical characteristic of the utilised material: AISI 304

The utilised material is the austenitic stainless steel widely adopted in biomedical applications: the AISI 304 stainless steel. The main mechanical characteristics are listed in Table 2.

<b>Young modulus (E)</b>	<b>190 GPa</b>
<b>Shear modulus</b>	<b>75 GPa</b>
<b>Poisson modulus</b>	<b>0.29</b>
<b>Yield stress (<math>\sigma_0</math>)</b>	<b>206.8 MPa</b>

Table 2. Mechanical properties of the AISI 304 stainless steel.

The material constitutive law utilised in the computational simulations was a linear elastic model, with the indication of the yield stress ( $\sigma_0$ ) of the material. This simple type of material model is acceptable since the stress and strain values generated do not reach the yield point ( $\sigma_0; \varepsilon_0$ ) in any of the FEA analysis performed, and the deformation values are very small. Beyond a stress limit called yield stress, the slope of the stress-strain curve should be lower than that in the first phase where the material characteristic in the elastic range follows a line. The material linear elastic model used in this work is similar to the one shown in Figure 4.

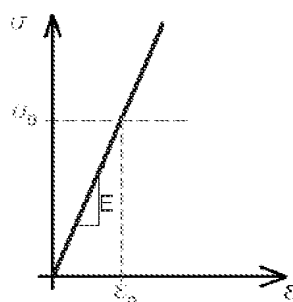


Figure 4. Characteristic linear elastic model of the material used in the simulations.

## 1.4 Quantities of interest

The aim of the simulation is to understand the different mechanical behaviour of notched hypotubes in the two versions described above in order to understand the potential benefits of "rounded" notches vs. "simple" notches.

From a *microscopic* point of view, it is universally acknowledged that the presence of rounded ends on the notches causes less crack generation in metallic materials and usually, as a consequence, a better fatigue resistance of components. Nevertheless this is not very important in this case, since a hypotube mounted on a medical device used for intravascular treatments (as the one analysed in this case) rarely undergoes cyclic stresses during its usage.

It is much more important to investigate the *overall performances* of the hypotubes in their whole, in terms of the component trackability, its flexibility and its torque response. In order to do this, the mechanical behaviour of a distal portion of the two different hypotubes has been analysed in terms of:

1. static linear elastic response to compressive and traction forces (applied among the longitudinal axis of the hypotube);
2. static linear elastic response to bending moment;
3. static linear elastic response to torque moment.

For each simulation the commercial software 'Simulation Xpress' (Dassault Systèmes SolidWorks Corporation) has been used to perform static linear elastic analysis with the following calculated outputs:

- The maximum value of the Von Mises stress, a scalar stress value which can be used to predict the yielding of ductile materials, such as AISI 304 stainless steel. It can be assumed that the hypotube will start yielding when its von Mises stress reaches the AISI 304 yield stress  $\sigma_0$ . Below this value, material response is assumed to be elastic. The maximum Von Mises stress value gives an indication about the mechanical resistance of the device, when it undergoes the defined forces/moment.
- The maximum value of  $U_{res}$ , a scalar defined as the norm of the displacement vector, as defined below:

$$\text{Displacement vector: } \vec{u} = (u_x; u_y; u_z)$$

$$U_{res} = \|u\| = \sqrt{u_x^2 + u_y^2 + u_z^2}$$

The maximum  $U_{res}$  value describes the maximum local deformation generated in the device by the forces/moment applied.

## 1.5 Description of the computational simulations

### 1.5.1 Static linear elastic response to compressive and traction forces (applied among the longitudinal axis of the hypotube):

Two simulations have been performed applying to the hypotube, among its longitudinal axis, the following forces (refer to Figure 4 below).

- $F = +2N$  force → positive value: traction force;
- $F = -2N$  force → negative value: compressive force.

As it is shown in Figure 5, the force has been applied to the proximal portion of the hypotube, while the distal surface has been fixed with an “encastre” boundary condition.

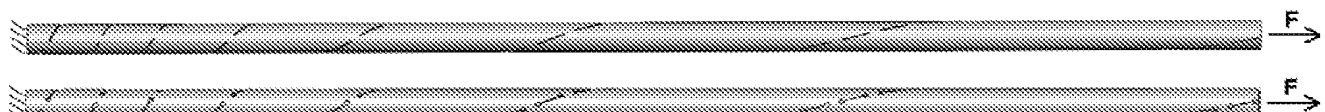


Figure 5. Forces and boundary conditions applied for compressive and traction elastic response analysis.

The chosen force value ( $F = \pm 2N$ ) is similar to the values measured during insertion and retraction of devices in the Invatec trackability validation bench tests; these tests are performed under experimental conditions that reproduce the clinical intended use of the considered medical device. Moreover, in the static linear elastic analysis performed, the chosen force value generates meaningful stress and strain values, since they are below the yield point defined in bullet point 1.3.

Finally, in both cases the maximum Von Mises and  $U_{res}$  values due to elastic deformation of the material have been calculated and plotted graphically.

### 1.5.2 Static linear elastic response to bending moment:

A simulation has been performed applying to the hypotube's proximal surface a bending force normal to the hypotube's longitudinal axis ( $T$ ) at distance ( $d$ ) from the distal surface fixed with an “encastre” boundary condition, as depicted in Figure 6 below: in the image only the “rounded-notches” hypotube version is represented, but the same force and boundary conditions have been applied to the “simple-notches” hypotube version.

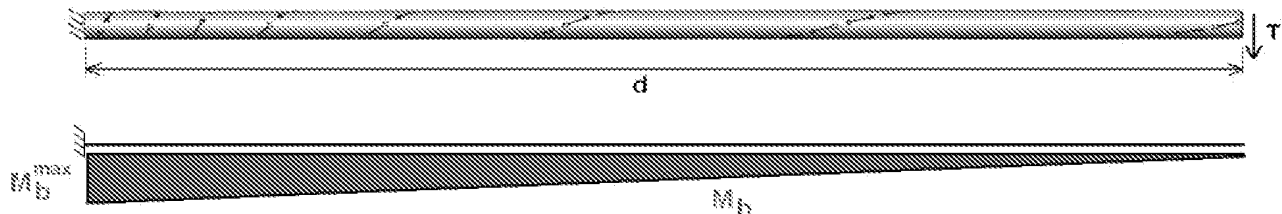


Figure 6. Forces and boundary conditions applied for bending moment elastic response analysis.

As shown in figure above, since  $T = 0.015\text{N}$  and  $d = 24.6\text{mm}$ , the maximum bending moment ( $M_b^{\max} = T \cdot d$ ) is located on the distal end of the hypotube, with a value of  $0.369 \text{ N}\cdot\text{mm}$ . Moreover, in the static linear elastic analysis performed, the chosen moment value generates meaningful stress and strain values, since they are below the yield point defined in bullet point 1.3.

Finally, in both cases the maximum Von Mises and  $U_{\text{res}}$  values due to elastic deformation of the material have been calculated and plotted graphically.

### 1.5.3 Static linear elastic response to torque moment:

A simulation has been performed applying to the hypotube's proximal surface a torque moment to the hypotube ( $M_t$ ) at distance ( $d$ ) from the distal surface fixed with an "encastre" boundary condition. In Figure 7 below only the "rounded-notches" hypotube version is represented, but the same boundary conditions have been applied to the "simple-notches" hypotube version.

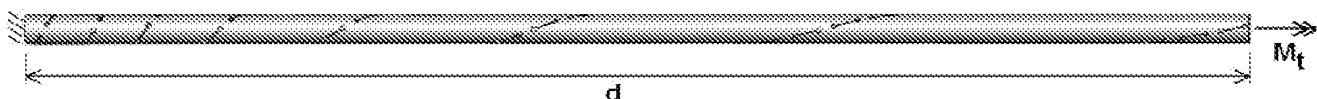


Figure 7. Forces and boundary conditions applied for torque moment elastic response analysis.

The maximum bending moment applied in the simulation has a value of  $M_t = 0.112 \text{ N}\cdot\text{mm}$ . Moreover, in the static linear elastic analysis performed, the chosen moment value generates meaningful stress and strain values, since they are below the yield point defined in bullet point 1.3.

Finally, in both cases the maximum Von Mises and  $U_{\text{res}}$  values due to elastic deformation of the material have been calculated and plotted graphically.

## 2. Results

### 2.1 Static linear elastic response to compressive and traction forces (applied among the longitudinal axis of the hypotube):

As regards the static linear elastic response to compressive and traction forces simulation, results are shown below.

#### 2.1.1 SIMPLE-NOTCHES VERSION HYPOTUBE:

##### RESPONSE TO COMPRESSIVE FORCES:

- Figure 8a: Von Mises maximum stress generated by compressive forces.  
→  $\sigma_{\text{Von Mises (MAX)}} = 142.7 \text{ MPa.}$
- Figure 8b: maximum local deformation generated by compressive forces.  
→  $U_{\text{res (MAX)}} = 2.89 \cdot 10^{-3} \text{ mm.}$

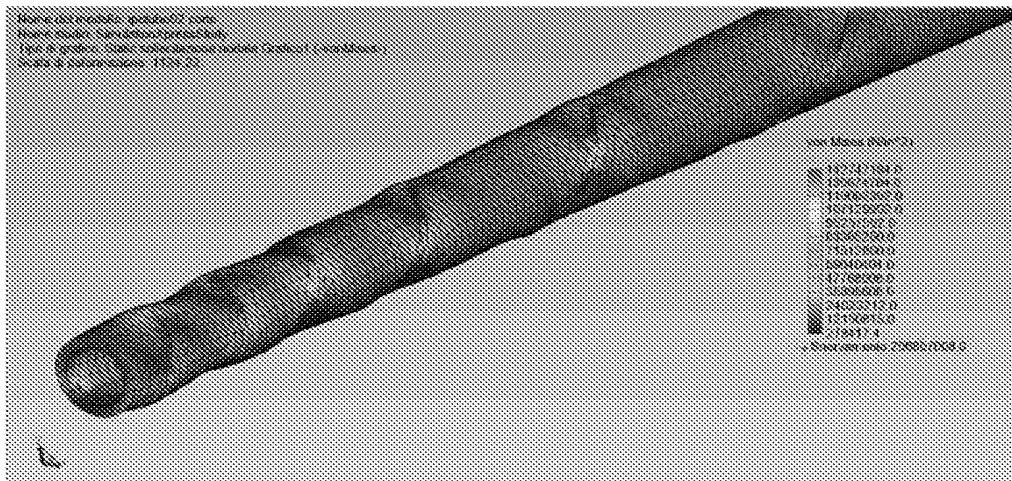


Figure 8a. Resultant Von Mises stress distribution in the static linear elastic response analysis to compressive forces.

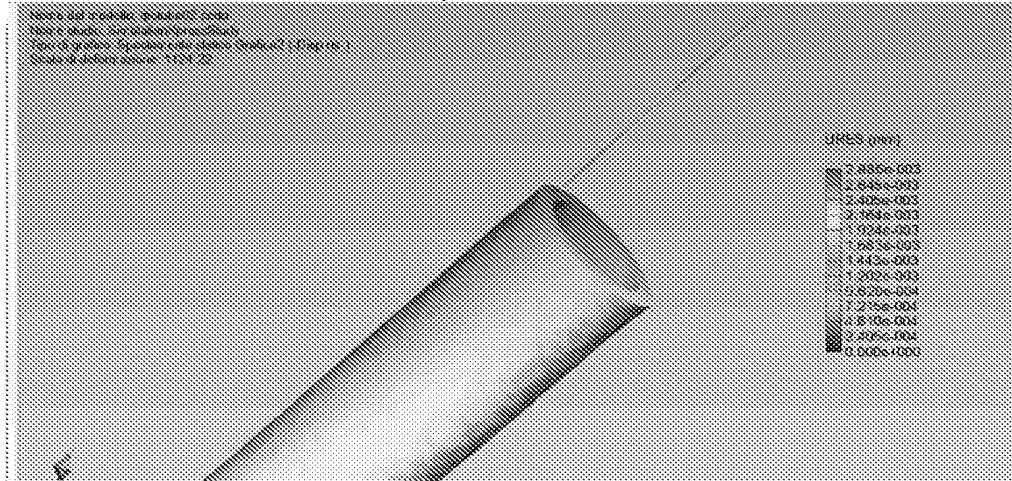


Figure 8b. Resultant maximum local deformation distribution in the static linear elastic response analysis to compressive forces.

## **RESPONSE TO TRACTION FORCES:**

- Figure 9a: Von Mises maximum stress generated by traction forces.  
→  $\sigma_{\text{Von Mises (MAX)}} = 142.8 \text{ MPa.}$
- Figure 9b: maximum local deformation generated by traction forces.  
→  $U_{\text{res (MAX)}} = 2.89 \cdot 10^{-3} \text{ mm.}$

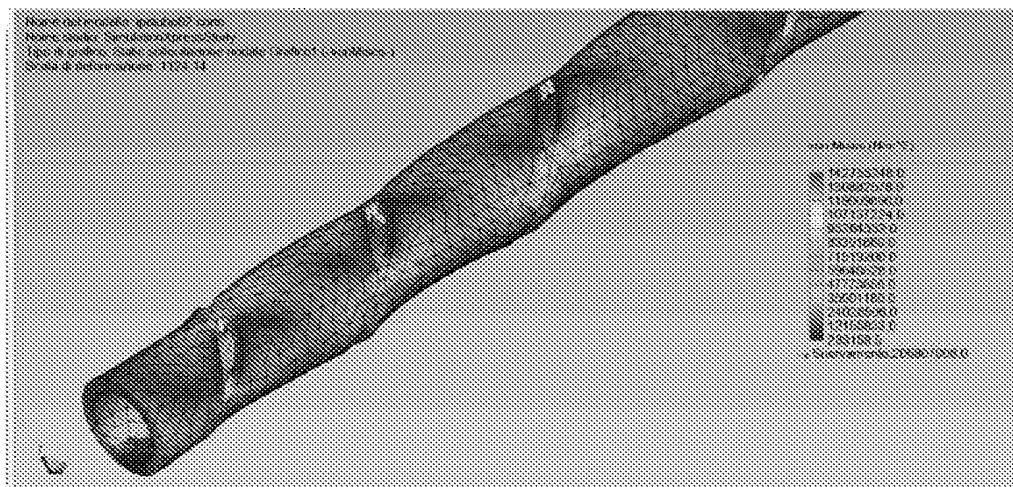


Figure 9a. Resultant Von Mises stress distribution in the static linear elastic response analysis to traction forces.

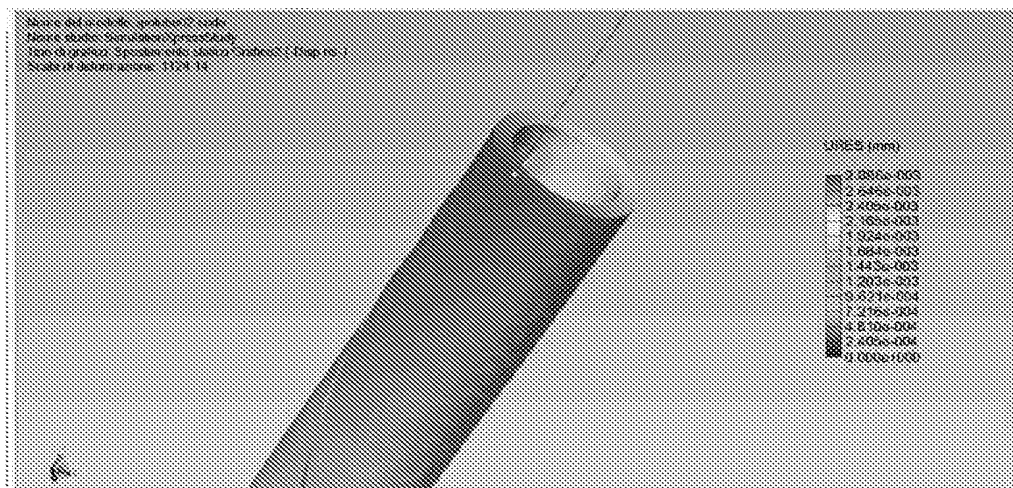


Figure 9b. Resultant maximum local deformation distribution in the static linear elastic response analysis to traction forces.

## **2.1.2 ROUNDED-NOTCHES VERSION HYPOTUBE: RESPONSE TO COMPRESSIVE FORCES:**

- Figure 10a: Von Mises maximum stress generated by compressive forces.  
 $\rightarrow \sigma_{\text{Von Mises (MAX)}} = 132.1 \text{ MPa.}$
- Figure 10b: maximum local deformation generated by compressive forces.  
 $\rightarrow U_{\text{res (MAX)}} = 3.66 \cdot 10^{-3} \text{ mm}$

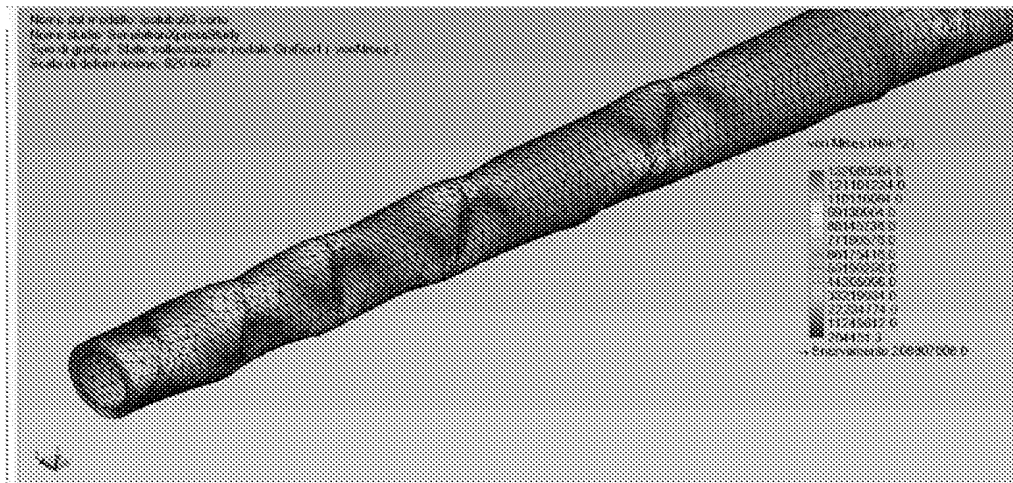


Figure 10a. Resultant Von Mises stress distribution in the static linear elastic response analysis to compressive forces.

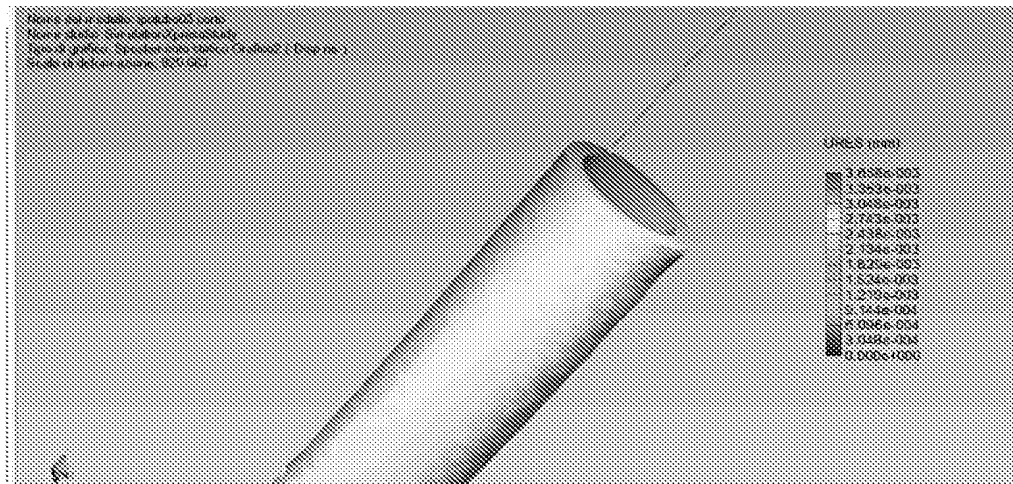


Figure 10b. Resultant maximum local deformation distribution in the static linear elastic response analysis to compressive forces.

## **RESPONSE TO TRACTION FORCES:**

- Figure 11a: Von Mises maximum stress generated by traction forces.  
→  $\sigma_{\text{Von Mises (MAX)}} = 132.1 \text{ MPa.}$
- Figure 11b: maximum local deformation generated by traction forces.  
→  $U_{\text{res (MAX)}} = 3.66 \cdot 10^{-3} \text{ mm.}$

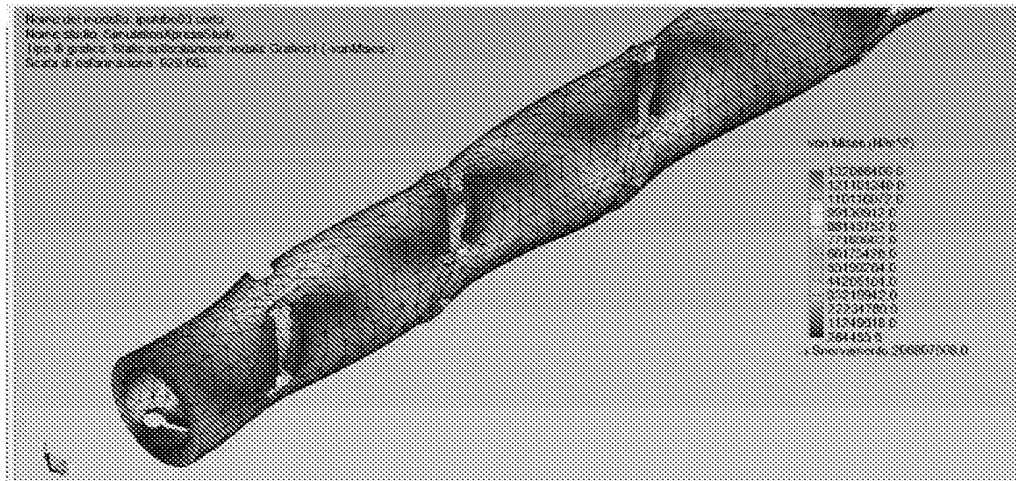


Figure 11a. Resultant Von Mises stress distribution in the static linear elastic response analysis to traction forces.

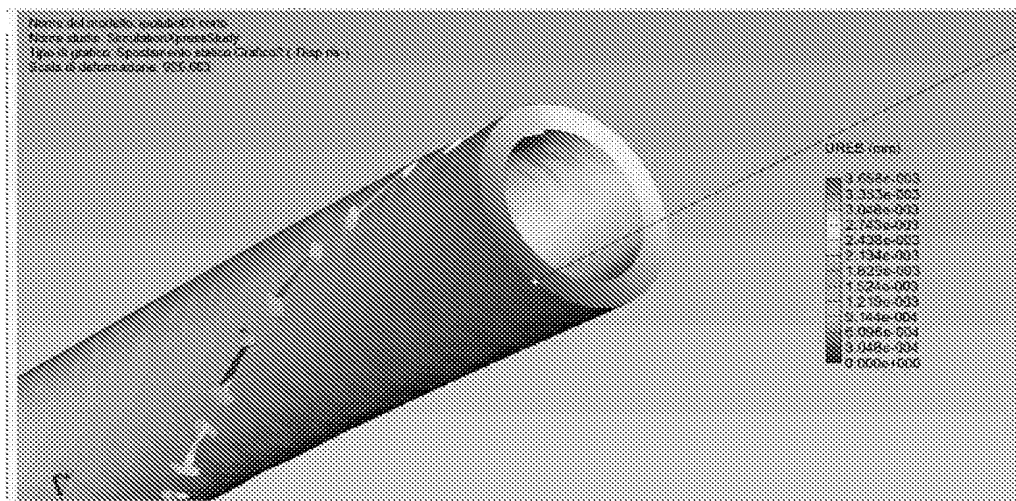


Figure 11b. Resultant maximum local deformation distribution in the static linear elastic response analysis to traction forces.

## **2.2 Static linear elastic response to bending moment:**

As regards the static linear elastic response to bending moment simulation, results are shown below.

### **2.2.1 SIMPLE-NOTCHES VERSION HYPOTUBE:**

- Figure 12a: Von Mises maximum stress generated by bending moment.  
→  $\sigma_{\text{Von Mises (MAX)}} = 155.5 \text{ MPa.}$
- Figure 12b: maximum local deformation generated by bending moment.  
→  $U_{\text{res (MAX)}} = 0.096 \text{ mm.}$

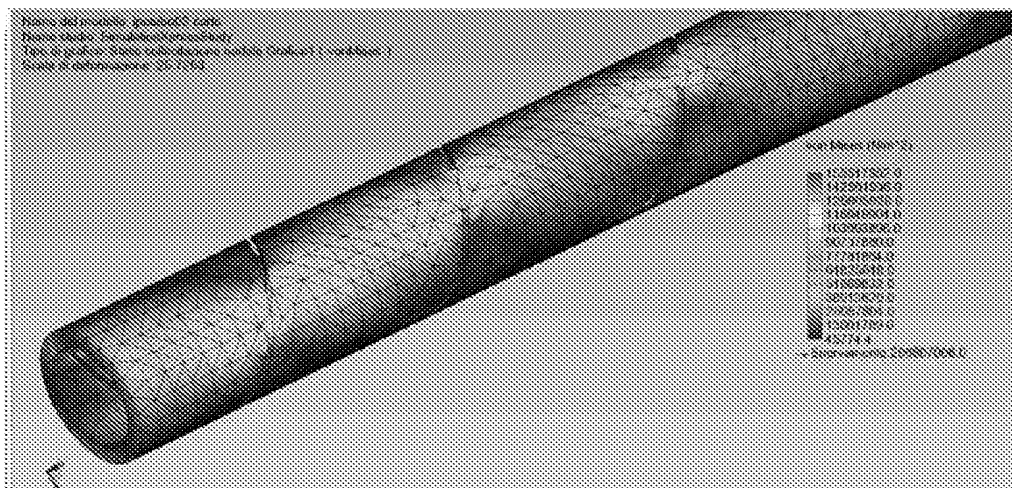


Figure 12a. Resultant Von Mises stress distribution in the static linear elastic response analysis to bending moment.

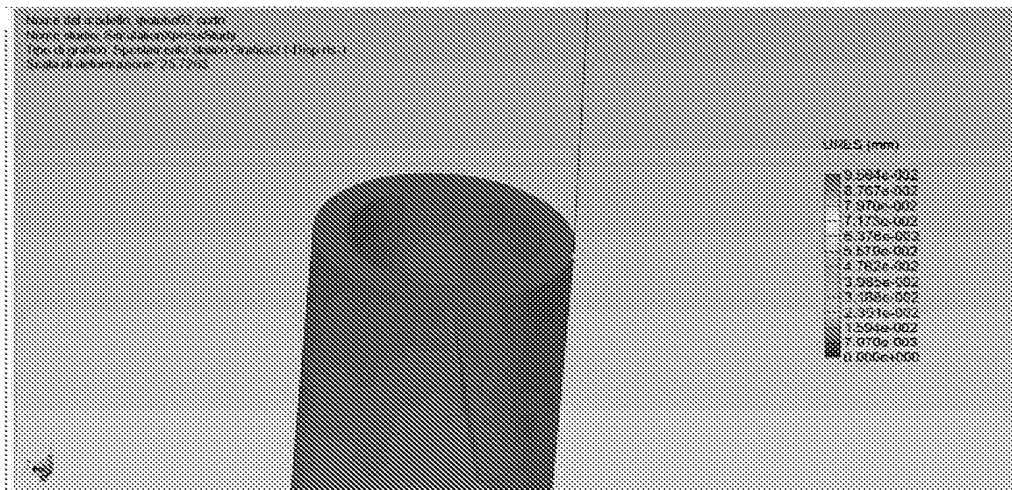


Figure 12b. Resultant maximum local deformation distribution in the static linear elastic response analysis to bending moment.

### **2.2.2 ROUNDED-NOTCHES VERSION HYPOTUBE:**

- Figure 13a: Von Mises maximum stress generated by bending moment.  
→  $\sigma_{\text{Von Mises (MAX)}} = 172.6 \text{ MPa.}$
- Figure 13b: maximum local deformation generated by bending moment.  
→  $U_{\text{res (MAX)}} = 0.110 \text{ mm}$

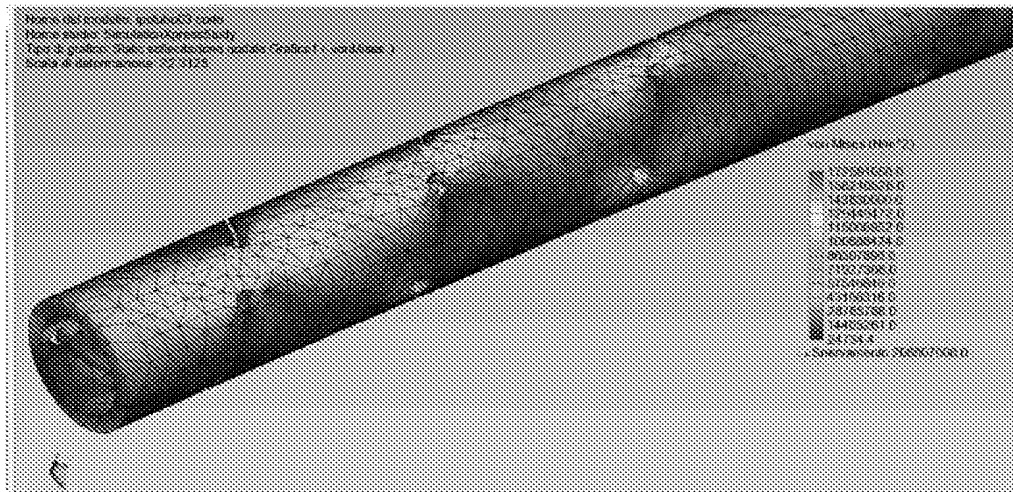


Figure 13a. Resultant Von Mises stress distribution in the static linear elastic response analysis to bending moment.

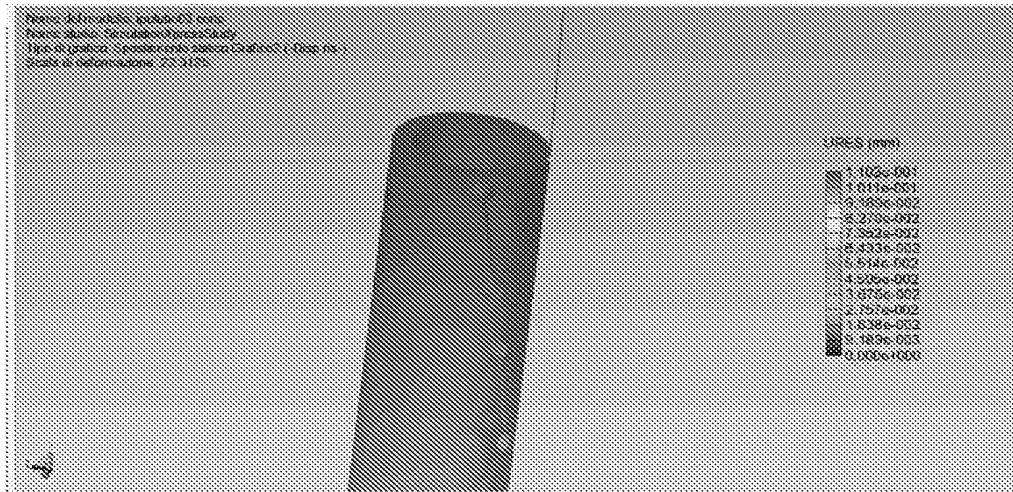


Figure 13b. Resultant maximum local deformation distribution in the static linear elastic response analysis to bending moment.

## 2.3 Static linear elastic response to torque moment:

As regards the static linear elastic response to torque moment simulation, results are shown below.

### 2.3.1 SIMPLE-NOTCHES VERSION HYPOTUBE:

- Figure 14a: Von Mises maximum stress generated by torque moment.  
→  $\sigma_{\text{Von Mises (MAX)}} = 78.8 \text{ MPa}$ .
- Figure 14b: maximum local deformation generated by torque moment.  
→  $U_{\text{res (MAX)}} = 1.59 \cdot 10^{-3} \text{ mm}$ .

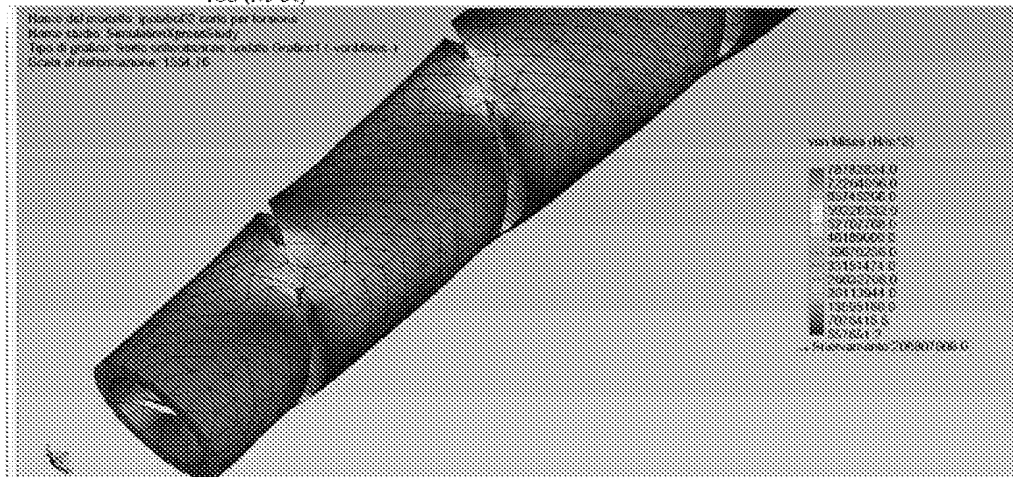


Figure 14a. Resultant Von Mises stress distribution in the static linear elastic response analysis to torque moment.

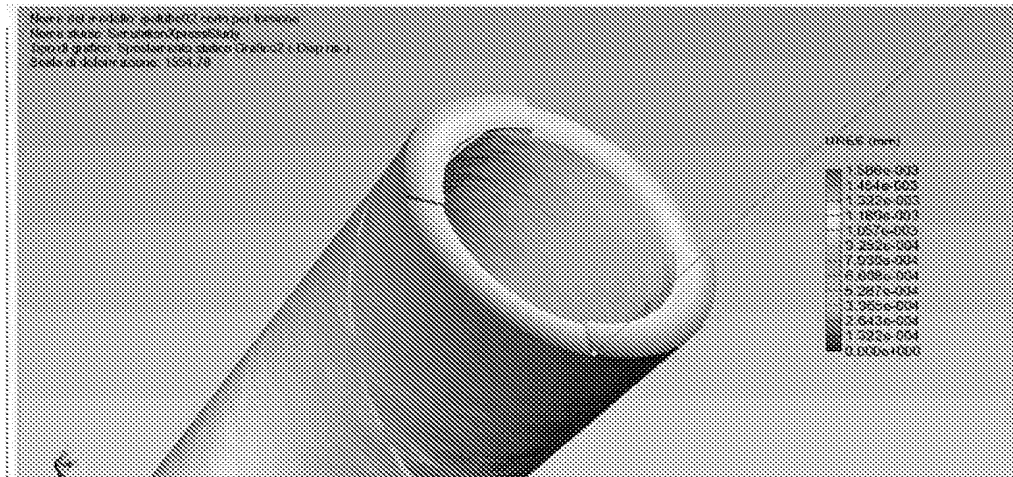


Figure 14b. Resultant maximum local deformation distribution in the static linear elastic response analysis to torque moment.

### **2.3.2 ROUNDED-NOTCHES VERSION HYPOTUBE:**

- Figure 15a: Von Mises maximum stress generated by torque moment.  
→  $\sigma_{\text{Von Mises (MAX)}} = 60.5 \text{ MPa}$ .
- Figure 15b: maximum local deformation generated by torque moment.  
→  $U_{\text{res (MAX)}} = 1.87 \cdot 10^{-3} \text{ mm}$

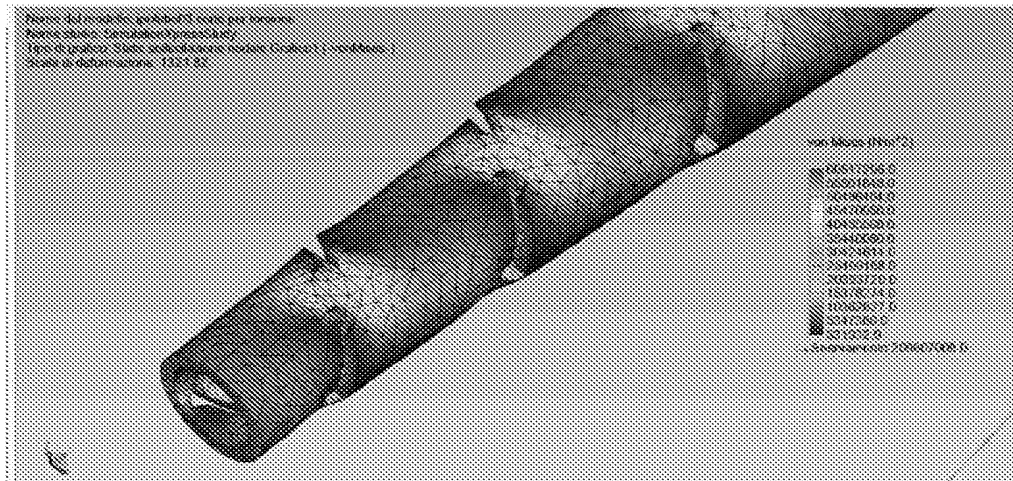


Figure 15a. Resultant Von Mises stress distribution in the static linear elastic response analysis to torque moment.

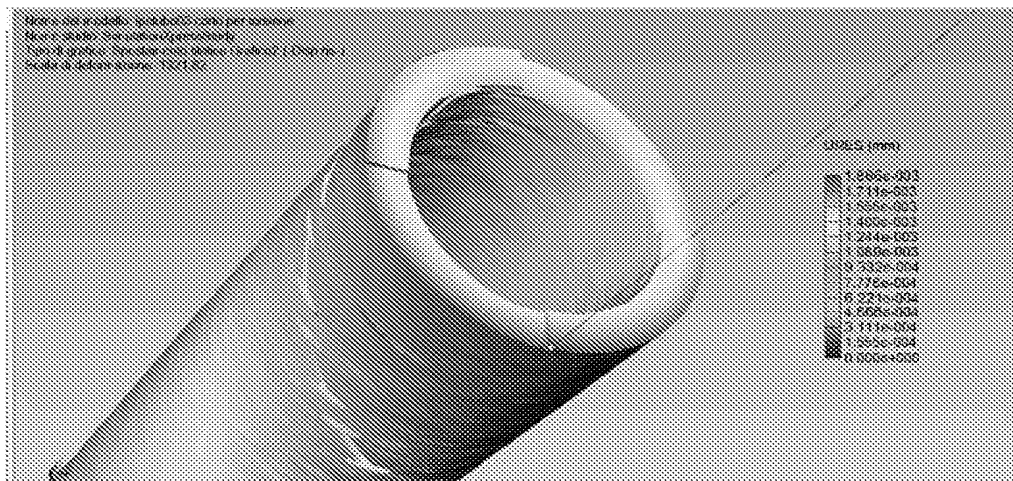


Figure 15b. Resultant maximum local deformation distribution in the static linear elastic response analysis to torque moment.

The quantities of interest for the mechanical characterization of the two different versions of the hypotube ("simple-" and "rounded-notches") can be summarized in Table 3.

	"SIMPLE-NOTCHES"		"ROUNDED-NOTCHES"	
	$\sigma_{\text{Von Mises (MAX)}} [\text{MPa}]$	$U_{\text{res (MAX)}} [\text{mm}]$	$\sigma_{\text{Von Mises (MAX)}} [\text{MPa}]$	$U_{\text{res (MAX)}} [\text{mm}]$
COMPRESSIVE FORCES	142.7	$2.89 \cdot 10^{-3}$	132.1	$3.66 \cdot 10^{-3}$
TRACTION FORCES	142.8	$2.89 \cdot 10^{-3}$	132.1	$3.66 \cdot 10^{-3}$
BENDING MOMENT	155.5	0.096	172.6	0.110
TORQUE MOMENT	78.6	$1.59 \cdot 10^{-3}$	60.5	$1.87 \cdot 10^{-3}$

Table 3. Comparison of the "simple-notches" and "rounded-notches" versions of the hypotube.

We hereby declare that all statements made herein of our own knowledge are true, and that all statements made on information and belief are believed to be true; and further that these statements are made with the knowledge that the making of willful false statements or the like is punishable by fine or imprisonment, or both, under Section 1001 of Title 18 of the United States Code and that such willful false statements may jeopardize the validity of the application or any patents issued thereon.

January , 2010

(date)

Achille Sina

January , 2010

(date)

Marco Milani

## **Appendix "A"**

**Name:** Achille Sina

**Education:** Industrial Mechanical certificate

### **Job experience:**

- **Company:** Invatec S.p.A. – Roncadelle, BS, Italy. (Jan. 1999 – actual)
  - **Role:** Project Leader
  - **Dept.:** Research & Development
  - **Main activities:** Project leader of catheters Percutaneous Transluminal Coronary Angioplasty (PTCA) and Percutaneous Transluminal Angioplasty (PTA). Feasibility and prototype of new products. Bench test with competitors. Compliant analysis.
- **Company:** Fogazzi S.r.l. – Concesio, BS, Italy. (Jan. 1996 – Jan. 1999)
  - **Role:** Project Leader
  - **Dept.:** Research & Development
  - **Main activities:** Project leader in medical device company. Engineering process and new products developer.

## Appendix "B"

**Name:** Marco Miliani

**Education:** Master Degree in Biomedical Engineering (Oct. 2005)

**University:** 'Politecnico di Milano' (Milan - Italy)

### Job experience:

- **Company:** Invatec S.p.A. – Roncadelle, BS, Italy. (Jun. 2008 – actual)
  - **Role:** Project Leader
  - **Dept.:** Research & Development
  - **Main activities:** Design and project management; definition and development of cardio-vascular biomedical devices (intra-vascular catheters).
- **Company:** Prodent Italia S.r.l. – Pero, MI, Italy. (Dec. 2007 – Jun. 2008)
  - **Role:** Design Engineer
  - **Dept.:** Research & Development
  - **Main activities:** Design and project management; definition and development of dental implants and other surgical instruments used for implantation and bone reconstruction. Component design supported by Finite Element Modelling.
- **Company:** Siemens S.p.A. – Milan, Italy. (Jan. 2006 – Dec. 2007)
  - **Role:** Application Specialist
  - **Dept.:** Medical Solutions
  - **Main activities:** Technical on-field support for diagnostic imaging in angiographic cath labs: image processing and technical settings for enhanced image quality.
- **Institute:** 'Politecnico di Milano' University. (Sept. 2004 – Dec. 2005)
  - **Role:** Research Fellow
  - **Dept.:** Structural Engineering Department – Laboratory of Biological Structure Mechanics (*LaBS*).
  - **Main activities:** Finite Element Modelling of medical devices (total knee replacement prosthesis, total hip replacement prosthesis, dental implants). Mathematical modelling for wear phenomena in artificial joints. Design of mechanical devices used for bench testing activities (fatigue testing).

### F.E.M. experience:

- Structural linear and non-linear analysis.
- Elastic, elasto-plastic material models.
- Dynamic, time-dependent loading.
- Standard and Explicit formulation.
- Contact and friction modeling.

**Claims of application 10/531466**

20. Tube, in particular for the use in medical devices in the form of catheters for endoluminal operations, comprising in at least one portion of its wall notches having a width A such as to locally increase flexibility of said tube, said notches being provided in at least one distal zone of said tube and exhibiting a substantially discontinuous helical pattern, wherein said notches form an angle  $\alpha$  with a circumference obtained on an outside surface of said tube, said angle  $\alpha$  increasing continuously from a distal end in a proximal direction, wherein each of said notches has two ends and a hole, having a diameter greater than the width of the notch, is formed at each said end to relieve stresses.
21. Tube according to claim 20, wherein said notches having a predetermined axial distance from one another.
22. Tube according to claim 21, wherein said axial distance between said notches increases from the distal end in the proximal direction.
23. Tube according to claim 20, wherein a width of said angle  $\alpha$  increases by an amount  $\beta$  at each arc  $\gamma$  covered on the surface of the tube in terms of width E of each said notch and of angular distance G between two consecutive said notches.
24. Tube according to claim 23, wherein a measure of said arc  $\gamma$  is between 0° and 360°.
25. Tube according to claim 20, wherein said width A is between 5  $\mu\text{m}$  and 1 mm.
26. Tube according to claim 20, wherein said width A is between 10  $\mu\text{m}$  and 25  $\mu\text{m}$ .
27. (canceled)

28. Tube according to claim 20, wherein said portion comprising said notches extends from said distal end in a proximal direction for a length of between 70 and 110 mm.
29. Tube according to claim 20, wherein said portion comprising said notches extends from said distal end in a proximal direction for a length of between 80 and 100 mm.
30. Tube according to claim 20, wherein said tube is realized with a metal material.
31. Tube according to claim 30, wherein said metal material is stainless steel.
32. Tube according to claim 20, wherein said tube is made of a polymeric material.
33. Tube according to claim 20, wherein said tube is made of a composite material.
34. Tube according to claim 20, wherein said surface of said tube is covered with a layer of polytetrafluoroethylene (PTFE).
35. Catheter for endoluminal operations comprising a tube according to claim 20.